miR-132/212 Modulates Seasonal Adaptation and Dendritic Morphology of the Central Circadian Clock.

Lucia Mendoza-Viveros, Cheng-Kang Chiang, Jonathan L.K. Ong, Sara Hegazi, Arthur Cheng, Pascale Bouchard-Cannon, Michael Fana, Christopher Lowden, Peng Zhang, Béatrice Bothorel, et al.

Article

Cell Reports

miR-132/212 Modulates Seasonal Adaptation and Dendritic Morphology of the Central Circadian Clock

Graphical Abstract

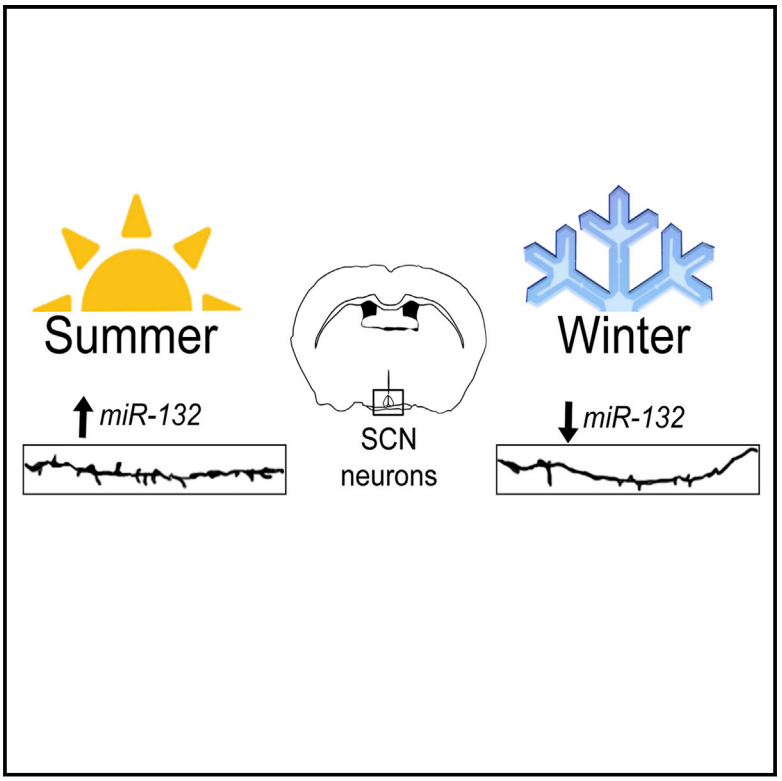

Authors

Lucia Mendoza-Viveros, Cheng-Kang Chiang, Jonathan L.K. Ong, ..., Valérie Simonneaux, Daniel Figeys, Hai-Ying M. Cheng

Correspondence

haiying.cheng@utoronto.ca

In Brief

Seasonal adaptation is believed to require plasticity in the SCN, although the mechanisms are unclear. Mendoza-Viveros et al. report that miR-132/212 modulates dendritic protrusion density and photoperiodic adaptation in mice and hamsters, by regulating the expression of MeCP2, and downstream BDNF and mTOR signaling.

Highlights

- miR-132/212 modulates entrainment to seasonal photoperiods
- Ablation of miR-132/212 reduces dendritic spine density of SCN clock neurons
- Photoperiod regulates miR-132/212 expression and dendritic morphology in hamsters
- miR-132/212 acts through MeCP2, and downstream BDNF and mTOR are involved

Accession Numbers

PXD003635

Mendoza-Viveros et al., 2017, Cell Reports *19*, 505–520
April 18, 2017
http://dx.doi.org/10.1016/j.celrep.2017.03.057

Cell Reports
Article

miR-132/212 Modulates Seasonal Adaptation and Dendritic Morphology of the Central Circadian Clock

Lucia Mendoza-Viveros,[1,2] Cheng-Kang Chiang,[3] Jonathan L.K. Ong,[1] Sara Hegazi,[1,2] Arthur H. Cheng,[1,2] Pascale Bouchard-Cannon,[1,2] Michael Fana,[1,2] Christopher Lowden,[1,2] Peng Zhang,[1] Béatrice Bothorel,[4] Matthew G. Michniewicz,[1] Stephen T. Magill,[5] Melissa M. Holmes,[2,6] Richard H. Goodman,[5] Valérie Simonneaux,[4] Daniel Figeys,[3,7] and Hai-Ying M. Cheng[1,2,8,*]

[1]Department of Biology, University of Toronto Mississauga, 3359 Mississauga Road, Mississauga, ON L5L 1C6, Canada
[2]Department of Cell and Systems Biology, University of Toronto, 25 Harbord Street, Toronto, ON M5S 3G5, Canada
[3]Ottawa Institute of Systems Biology, Department of Biochemistry, Microbiology and Immunology, University of Ottawa, 451 Smyth Road, Ottawa, ON K1H 8M5, Canada
[4]Institut des Neurosciences Cellulaires et Intégratives, UPR CNRS 3212, Université de Strasbourg, 5 rue Blaise Pascal, 67084 Strasbourg, France
[5]Vollum Institute, Oregon Health and Science University, Portland, OR 97239, USA
[6]Department of Psychology, University of Toronto Mississauga, 3359 Mississauga Road, Mississauga, ON L5L 1C6, Canada
[7]Canadian Institute for Advanced Research, 180 Dundas Street West, Toronto, ON M5G 1Z8, Canada
[8]Lead Contact
*Correspondence: haiying.cheng@utoronto.ca
http://dx.doi.org/10.1016/j.celrep.2017.03.057

SUMMARY

The central circadian pacemaker, the suprachiasmatic nucleus (SCN), encodes day length information by mechanisms that are not well understood. Here, we report that genetic ablation of *miR-132/212* alters entrainment to different day lengths and non-24 hr day-night cycles, as well as photoperiodic regulation of *Period2* expression in the SCN. SCN neurons from *miR-132/212*-deficient mice have significantly reduced dendritic spine density, along with altered methyl CpG-binding protein (MeCP2) rhythms. In Syrian hamsters, a model seasonal rodent, day length regulates spine density on SCN neurons in a melatonin-independent manner, as well as expression of miR-132, miR-212, and their direct target, MeCP2. Genetic disruption of *Mecp2* fully restores the level of dendritic spines of *miR-132/212*-deficient SCN neurons. Our results reveal that, by regulating the dendritic structure of SCN neurons through a MeCP2-dependent mechanism, miR-132/212 affects the capacity of the SCN to encode seasonal time.

INTRODUCTION

Circadian clocks are ubiquitous biological timing systems that enable most organisms on Earth to keep track of solar time. The central pacemaker in mammals resides in the hypothalamic suprachiasmatic nucleus (SCN), a network of ~20,000 neuronal oscillators (Ralph et al., 1990; Stephan and Zucker, 1972). The SCN generates self-sustained, near-24 hr oscillations that coordinate peripheral tissue clocks, maintaining temporal order in behavioral and physiological processes (Ralph et al., 1990). Circadian time (CT) is encoded by a set of autoregulatory transcription-translation feedback loops (TTFLs), in which components of the positive limb (CLOCK, BMAL1) drive transcription of repressive elements in the negative limb (*period1/2*, *cryptochrome1/2*) (Kume et al., 1999; Gekakis et al., 1998). Retinal inputs convey light information to the molecular clock of the SCN, triggering changes in *Period* transcription (Shigeyoshi et al., 1997). Although SCN neurons can oscillate cell-autonomously (Welsh et al., 1995), they need to coordinate their activities within a network to respond properly to light inputs and to generate coherent outputs (Yamaguchi et al., 2003).

MicroRNAs (miRNAs) are recognized as important players in circadian regulation. These non-coding RNAs regulate gene expression via translational repression or mRNA degradation of target transcripts. Global disruption of miRNA biogenesis in mice accelerates the speed of the circadian clock (Chen et al., 2013). Previously, we showed that a specific miRNA, miR-132, is expressed in the SCN in a light-inducible fashion and negatively modulates light-evoked SCN clock resetting (Cheng et al., 2007; Alvarez-Saavedra et al., 2011). miR-132 is part of the miR-132/212 gene cluster, sharing an identical seed region with miR-212 (Wanet et al., 2012). The physiological significance of the *miR-132/212* gene locus with respect to circadian rhythms has not been examined until now.

Here we report that genetic ablation of *miR-132/212* in mice alters behavioral entrainment to seasonal photoperiods and non-24 hr day-night cycles, as well as photoperiodic regulation of *Period2* expression in the SCN. Proteomic analysis of miR-*132/212*-deficient SCN under short days suggested that temporal regulation of actin cytoskeleton-based processes is affected. Furthermore, SCN neurons from *miR-132/212*

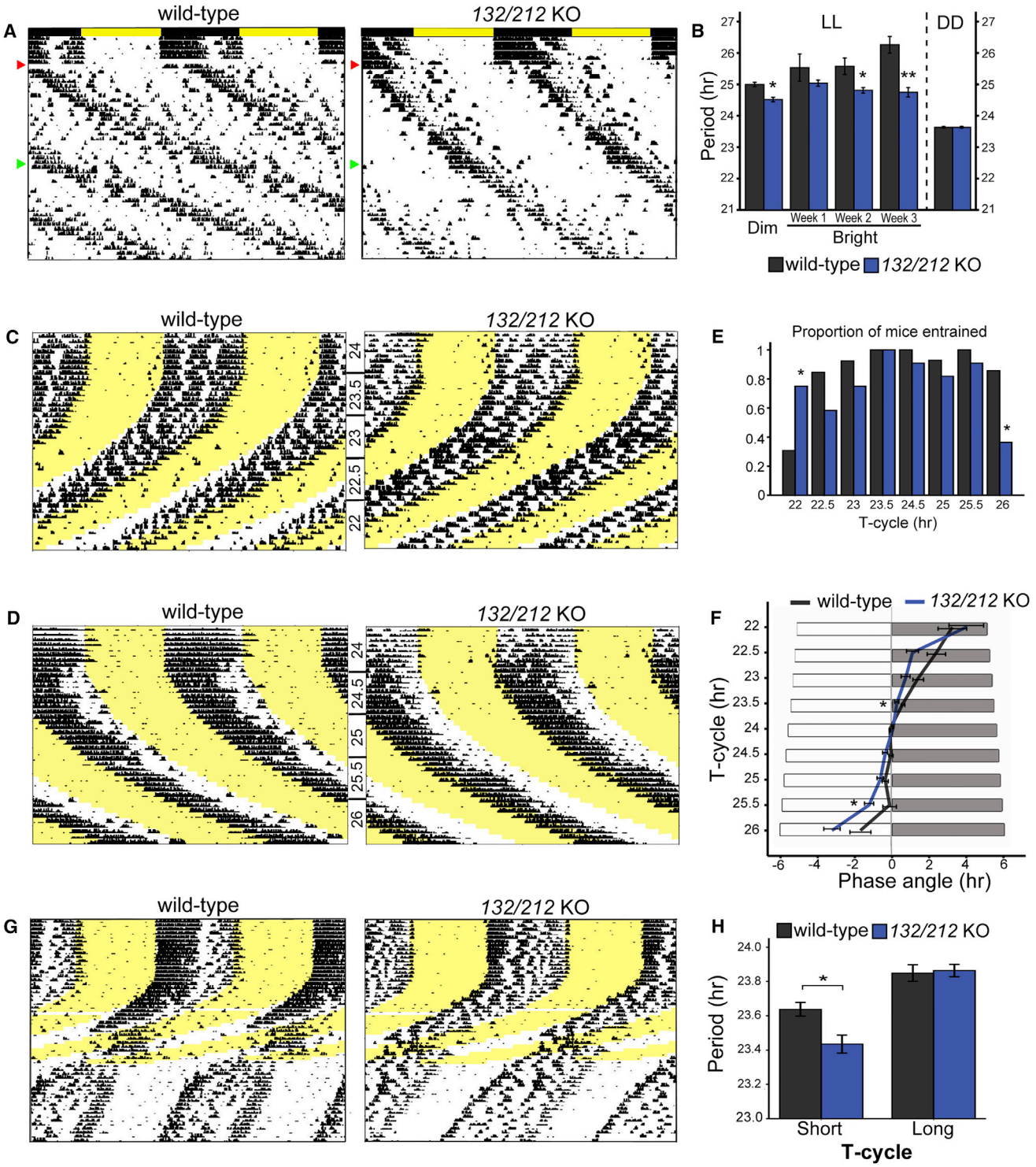

Figure 1. miR-132/212 Ablation Alters Behavioral Rhythms under Constant Light and Entrainment to Non-24 hr Light-Dark Cycles

(A) Representative actograms of wild-type and *132/212* KO mice following transfer to dim LL (30 lux, 0.38 μE; red arrowhead) and bright LL (100 lux, 1.24 μE; green arrowhead). Colored bars indicate the previous 12:12 hr L:D cycle.

(B) Period length under dim LL, bright LL, and DD conditions. Period lengths in the first, second, and third weeks of bright LL were measured separately. n = 10 per group in LL; n = 30 per group in DD.

(C and D) Representative actograms of wheel-running activities of wild-type and *132/212* KO mice that were subjected to stepwise (±0.5 hr) shortening or lengthening of the T-cycle from T24 to (C) T22 or (D) T26.

(legend continued on next page)

knockout (*132/212* KO) mice have a significant reduction in spine density under different photoperiods. Using Syrian hamsters as a model seasonal rodent, we found that spine density of SCN neurons is suppressed under short days in a melatonin-independent manner and that day length regulates the temporal expression of miR-132, miR-212, and their direct target, methyl CpG-binding protein (MeCP2). MeCP2 rhythms are perturbed in the SCN of *132/212* KO mice under different photoperiods, and genetic disruption of *Mecp2* fully restores spine density of *miR-132/212*-deficient SCN neurons. Altogether, our results reveal that *miR-132/212* regulates the dendritic structure of SCN neurons through a MeCP2-dependent mechanism and in doing so affects the ability of the SCN to encode day length.

RESULTS

miR-132/212 Regulates the Period-Lengthening Effects of Constant Light and the Intrinsic Molecular Rhythms of the SCN

Our previous studies suggested suppressive effects of miR-132 on light-induced phase shifts of behavioral rhythms (Cheng et al., 2007; Alvarez-Saavedra et al., 2011). Therefore, we constructed photic phase response curves (PRCs) to analyze clock resetting in mice bearing a germline deletion of miR-132 and miR-212 (Figures S1A and S1B). The PRCs for *132/212* KO and wild-type (WT) mice were indistinguishable (Figure S1B), as was the period of their behavioral rhythms under constant dark (DD) conditions (Figure 1B). However, when challenged with dim (30 lux, or 0.38 μE) and bright (100 lux, or 1.24 μE) constant light (LL), *132/212* KO mice had a significantly shorter period compared with WT animals (Figures 1A, 1B, and S1C). There was no difference between genotypes in the amplitude of LL rhythms (Figure S1D). These data suggest that miR-132/212 promotes the period-lengthening effects of constant light exposure but is dispensable for the determination of behavioral period under DD conditions and for acute photic resetting.

Despite the absence of a behavioral phenotype under DD conditions, *132/212* KO mice displayed perturbed molecular rhythms in the SCN. PER2 rhythms under DD conditions were significantly greater in amplitude in the SCN of *132/212* KO mice relative to WT (Figures S1F and S1I). Circadian expression of PER1 (Figures S1E and S1H) and BMAL1 (Figures S1G and S1J) were also perturbed in the absence of miR-132/212, albeit modestly in the case of PER1. The effects of *miR-132/212* ablation on PER2 rhythms were intrinsic to the SCN, because SCN explants from *132/212* KO pups bearing the PER2::LUCIFERASE knockin allele also showed a higher amplitude of PER2::LUC rhythms (Figures S1K and S1L). *miR-132/212*-deficient SCN explants had a significantly shorter intrinsic period relative to WT (Figure S1M), even though the behavioral period under DD conditions was similar between genotypes (Figure 1B). Altogether, these data suggest that miR-132/212 expression within the SCN modulates the intrinsic period and amplitude of molecular rhythms.

miR-132/212 Regulates Entrainment to Non-24 hr Day-Night Cycles

Given that *miR-132/212* ablation affects molecular rhythms and LL period, we re-examined the role of miR-132/212 in the clock entrainment process using a more challenging entrainment paradigm, the T-cycle (a non-24 hr light-dark [L:D] cycle). To entrain to a T-cycle, the clock of the animal must phase-shift each day, alter its period to approximate the T-cycle length, or both (Pittendrigh and Daan, 1976a, 1976b). T-cycle entrainment was tested by exposing T24 (12:12 hr L:D)-entrained mice to progressively longer or shorter T-cycles that eventually reached T26 (13:13 hr L:D) (Figure 1D) or T22 (11:11 hr L:D) (Figure 1C), respectively. Relative to WT controls, *132/212* KO mice had difficulty entraining to long T-cycles but entrained better to short T-cycles, as indicated by the proportion of entrained animals (Figure 1E). Those *132/212* KO mice that entrained to a long T-cycle (T25.5) did so with a significantly advanced phase angle relative to WT (i.e., daily activity onset markedly preceded dark onset) (Figure 1F). Furthermore, *132/212* KO mice had a shorter DD period than WT after exposure to T22 (Figures 1G and 1H) but were similar to WT after exposure to T26 (Figures 1H and S2A), indicating that miR-132/212 suppresses the long-lasting effects (i.e., circadian aftereffects) of shorter light cycles on behavioral period. Altogether, these data show that the absence of miR-132/212 enhances entrainment to short T-cycles and impairs entrainment to long T-cycles, the former partly because of a persistent change in circadian period.

miR-132/212 Regulates Photoperiodic Entrainment

Next, we investigated the role of miR-132/212 in entrainment to short (winter) and long (summer) photoperiods that, like entrainment to T-cycles, may involve plasticity of the SCN neuronal network (Meijer et al., 2010; Aton et al., 2004). *132/212* KO mice that were transitioned abruptly from 12:12 to 16:8 hr L:D (long day [LD]) required more days than WT animals to entrain stably to the long photoperiod (Figures 2B and 2C). Once entrained, *132/212* KO and WT mice exhibited a similar phase angle (Figure 2D). In contrast, although the speed of entrainment to 8:16 hr L:D (short day [SD]) was similar between genotypes (Figures 2A and 2C), the phase angle of *132/212* KO mice was markedly advanced relative to WT such that activity onset nearly coincided with dark onset (Figure 2D). Other parameters of locomotor activity were also assessed (Table S1). Overall, our data suggest that *miR-132/212* ablation enhances entrainment to short days but delays entrainment to long days.

Previous studies have suggested that the SCN adjusts to variations in day length by compressing the phase distribution

(E) Proportion of mice that remained entrained to the different T-cycles. n = 14 per group.
(F) Phase angle (in hours) of entrainment under different T-cycles. n = 14 per group.
(G) Representative actograms of wild-type and *132/212* KO mice that were subjected to a gradual shortening of the T-cycle by daily 10 min decrements from T24 to T22. Mice were released into DD once T22 was reached.
(H) Period aftereffects in mice subjected to a short (T22) or long (T26) T-cycle. n = 9 per group.
For (C), (D), and (G), periods of light are shaded in yellow. Values represent mean ± SEM. *$p < 0.05$ and **$p < 0.01$ versus wild-type.

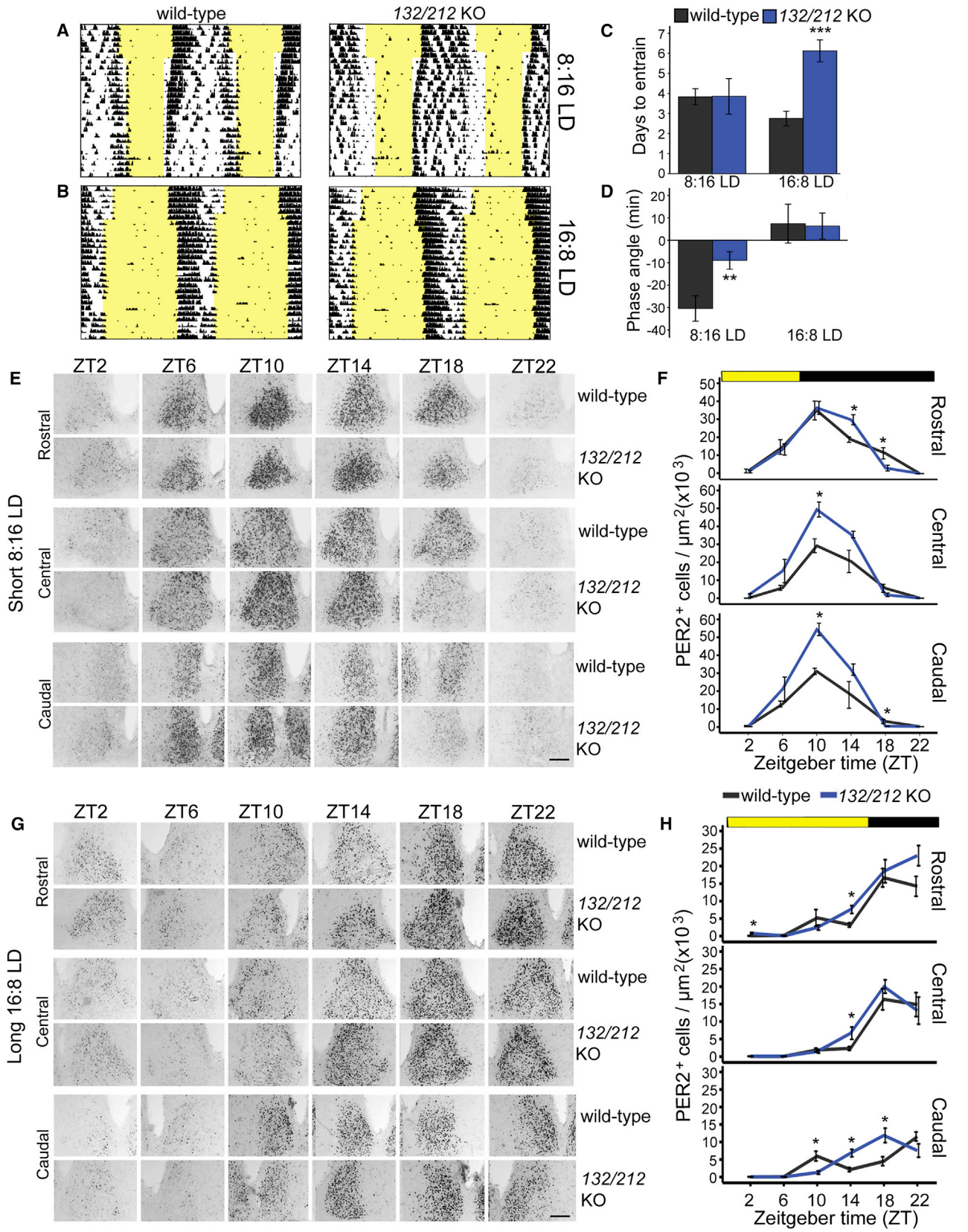

(legend on next page)

of individual neurons under short days and decompressing it under long days, as reflected in the pattern of *Per2* expression across the rostro-caudal axis of the SCN (Sosniyenko et al., 2009; VanderLeest et al., 2007; Hazlerigg et al., 2005). Under SD, PER2 expression across the rostro-caudal SCN axis peaked ~2 hr after dark onset, irrespective of genotype (Figures 2E and 2F). The amplitude of PER2 rhythms in the central and caudal, but not rostral, SCN was greater in SD-exposed *132/212* KO mice relative to WT (Figure 2F). Under LD, PER2 rhythms in the caudal SCN of WT mice were attenuated, broadened, and phase-advanced relative to the rostral and central SCN (Figures 2G and 2H). This phase separation between caudal and rostral-central SCN was not observed in LD-exposed *132/212* KO mice (Figure 2H). Furthermore, there was no difference in the amplitude of PER2 rhythms in the central SCN of LD-exposed *132/212* KO and WT mice (Figure 2H). Despite studies indicating that phase relationships between dorsal and ventral SCN might be altered by day length (Myung et al., 2015), we did not find differences in the phasing of PER2 oscillations between these two regions under all photoperiods tested in either genotype (data not shown). Collectively, our data suggest that photoperiod-dependent changes in spatiotemporal expression of PER2 in the SCN are modulated by miR-132/212.

miR-132/212 Shapes the Landscape of the Time-of-Day SCN Proteome under Short Days: Implications for Neuronal Structure

Next, we evaluated the time-of-day SCN proteome of SD-adapted *132/212* KO and WT mice using SILAC (stable isotope labeling by amino acids in cell culture)-based quantitative mass spectrometry (MS) to gain potential mechanistic insights (Figure 3A). One-way ANOVA revealed that 365 proteins (15.6% of quantified proteins) in the WT proteome showed significant temporal fluctuations, compared to 289 proteins (12.3%) in the *132/212* KO proteome (Figure 3B). Only 53 proteins were common to the time-of-day proteomes of WT and *132/212* KO SCN tissues (Figure 3B). Time-of-day-dependent expression of most proteins within the WT proteome was dampened or disrupted in the *132/212* KO proteome (Figure 3D), and vice versa (Figure 3E). The most highly represented biological processes (BPs) within the set of 312 proteins unique to the time-of-day WT proteome were (actin) cytoskeleton organization, actin filament-based processes, establishment or maintenance of cell polarity, and regulation of transcription (Figure 3C). In contrast, these biological processes were not enriched in the set of 236 proteins unique to the time-of-day *132/212* KO proteome (Figure 3C). These data suggest that *miR-132/212* ablation may have structural consequences resulting from altered temporal regulation of the cytoskeleton.

Pathway mapping revealed that the top three canonical pathways that were highly represented in the time-of-day WT proteome were EIF2 signaling, regulation of eIF4 and p70S6K signaling, and mTOR signaling (Figure 3F). In contrast, mTOR signaling and regulation of eIF4 and p70S6K signaling were not present in the top ten canonical pathways from the *132/212* KO dataset (Figure 3F). To validate the effects of *miR-132/212* ablation on the mTOR pathway, we analyzed the expression of phospho-S6 (p-S6) ribosomal protein, a marker of mTOR activity, in the SCN under three photoperiods (Figures 3G–3J, S3E, and S3F). Consistent with the MS data, the amplitude of p-S6 rhythms under 8:16 hr L:D was reduced in the *132/212* KO SCN relative to WT (Figures 3G and 3I). We also observed perturbation of p-S6 levels in the *132/212* KO SCN under 12:12 hr L:D (Figures S3E and S3F) but no difference between genotypes under 16:8 hr L:D (Figures 3H and 3J). Despite this, *miR-132/212* ablation did not have a global and uniform effect on protein synthesis in the SCN, as was evident when we compared the relative abundance of proteins that were significantly altered between the two genotypes (Figure S3D).

Collectively, our data indicate that *miR-132/212* ablation substantially alters the time-of-day SCN proteome of SD-exposed mice. miR-132/212 is important for maintaining high-amplitude rhythms of mTOR signaling in the SCN under short days. Our proteomic analysis further suggests that neuronal structure or morphology within the SCN may be compromised in the absence of miR-132/212.

miR-132/212 Deficiency Reduces Dendritic Spine Density of SCN Neurons

Previous studies have implicated miR-132 in the regulation of hippocampal dendritic complexity and spine formation (Magill et al., 2010; Wayman et al., 2008). To determine whether *miR-132/212* ablation affects dendritic morphology in the SCN, we used Golgi-Cox staining to analyze the density of various types of dendritic protrusions on SCN neurons of *132/212* KO and WT mice maintained under different photoperiods (Figures 4A–4G and S4A–S4D). *miR-132/212* ablation had a suppressive effect on total protrusion and simple spine density in a manner dependent on the photoperiod, time of day, and SCN region. In the central SCN, both parameters were significantly reduced in *132/212* KO mice relative to WT: (1) under 8:16 hr L:D regardless of time of day, (2) in the day only under 16:8 hr L:D, and (3) in the night only under 12:12 hr L:D (Figures 4D and 4E). Total protrusion and simple spine density were not affected in the caudal SCN of *132/212* KO mice but were reduced in the rostral SCN in the day only under 12:12 and 16:8 hr L:D (Figures S4B and S4C). The density of other

Figure 2. miR-132/212 Ablation Enhances Entrainment to Winter-like Photoperiods but Slows Re-entrainment to Summer-like Photoperiods

(A and B) Representative actograms of wild-type and *132/212* KO mice following transfer from 12:12 hr L:D to (A) 8:16 hr L:D or (B) 16:8 hr L:D. Periods of light are shaded in yellow.

(C) Days to re-entrain stably to the new photoperiod. n = 8 per group.

(D) Phase angle (in minutes) of entrainment under 8:16 or 16:8 hr L:D. n = 8 per group.

(E–H) Representative micrographs of PER2 immunoreactivity (IR) in the rostral, central, and caudal SCN of wild-type and *132/212* KO mice as a function of zeitgeber time (ZT) under (E) 8:16 hr L:D or (G) 16:8 hr L:D. ZT 0 is defined as lights on. Scale bar, 100 μm. Density of PER2-positive cells in the rostral, central, and caudal SCN of mice under (F) 8:16 hr L:D or (H) 16:8 hr L:D. n = 3–4 per group.

All values represent mean ± SEM. *p < 0.05, **p < 0.01, and ***p < 0.001 versus wild-type.

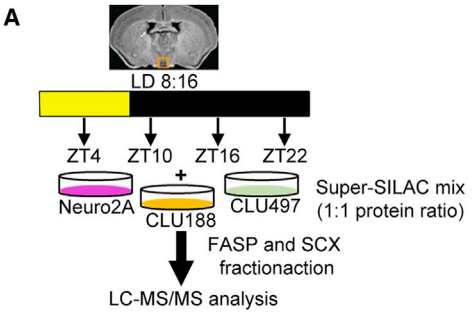

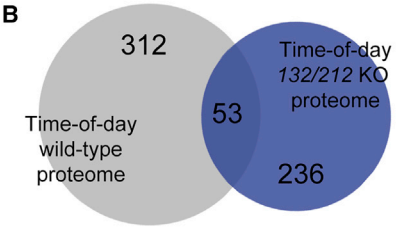

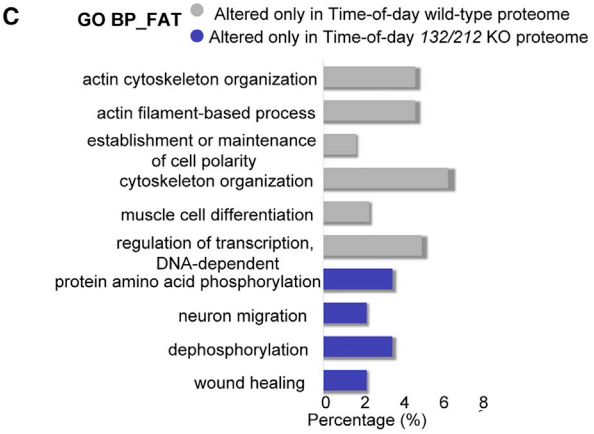

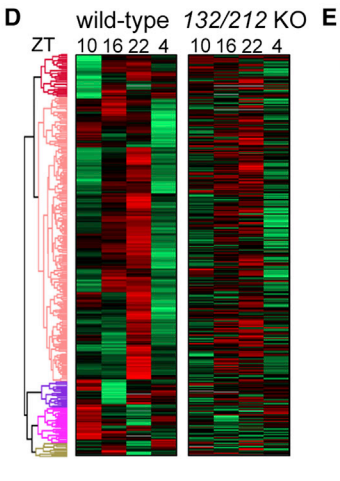

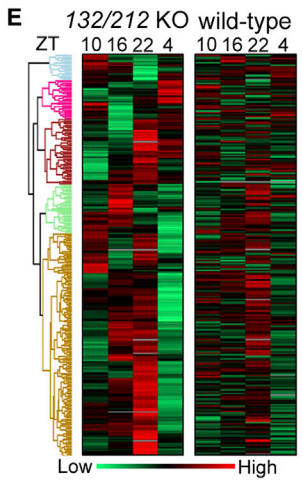

F

Ranking	Time-of-day wild-type proteome: Enriched canonical pathways	-log (p-value)	Time-of-day *132/212* KO proteome: Enriched canonical pathways	-log (p-value)
1	EIF2 Signaling	8.75	Breast Cancer Regulation by Stathmin1	9.13
2	Regulation of eIF4 and p70SK Signaling	8.52	Protein Kinase A Signaling	7.96
3	mTOR Signaling	6.93	Remodeling of Epithelial Adherent Junctions	7.81
4	Remodeling of Epithelial Adherens Junctions	6.87	Mitocondrial Dysfunction	7.66
5	RhoGDI Signaling	6.62	EIF2 Signaling	7.66
6	Motochondrial Dysfunction	6.35	RhoGDI Signaling	6.24
7	Clathrin-mediated Endocytosis Signaling	6.35	Integrin Signaling	5.67
8	PI3K/AKT Signaling	5.93	Relaxin Signaling	5.55
9	Protein Ubiquitination Pathway	5.92	Oxidative Phosphotylation	5.5
10	Signaling by Rho Family GTPases	5.79	Ephrin Receptor Signaling	5.49

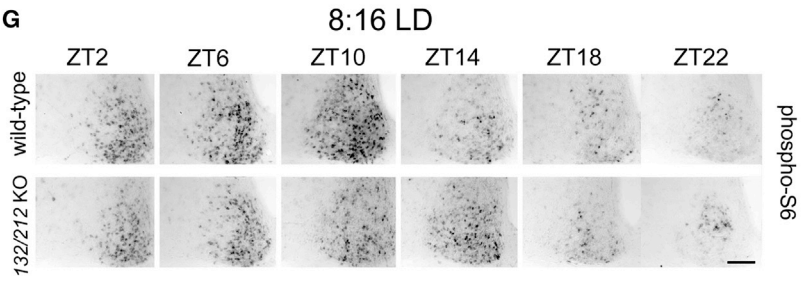

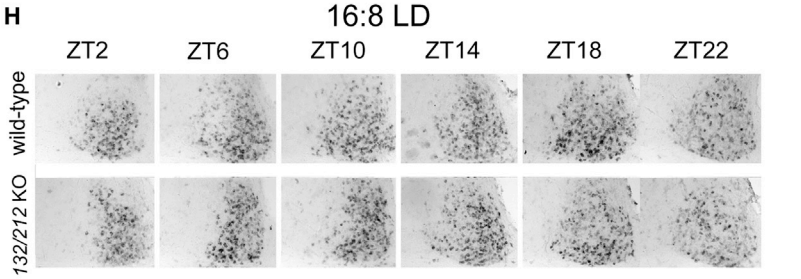

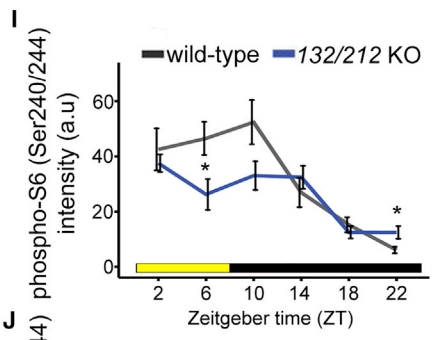

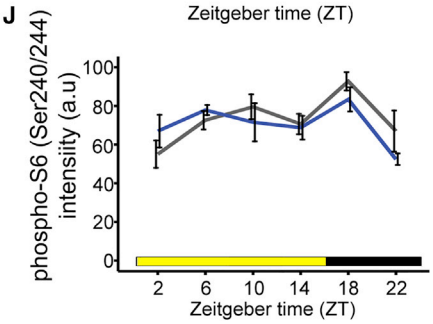

(legend on next page)

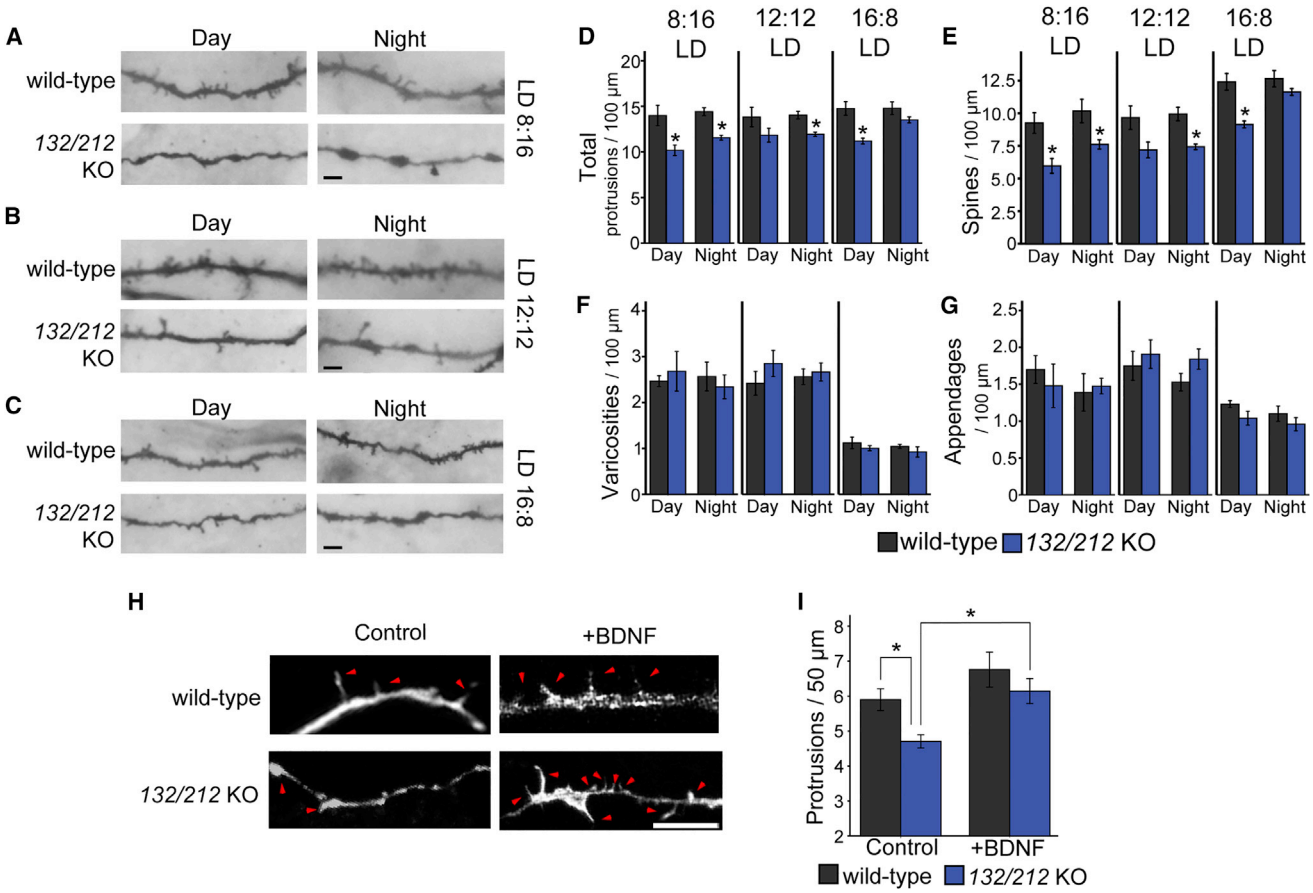

Figure 4. miR-132/212 Ablation Reduces Dendritic Spine Density of SCN Neurons

(A–C) Golgi-stained SCN neurons from wild-type and *132/212* KO mice maintained under (A) 8:16 hr L:D, (B) 12:12 hr L:D, or (C) 16:8 hr L:D. Tissues were harvested in the middle of the day or night. Scale bar, 10 μm.

(D–G) Density of (D) total protrusions, (E) simple spines, (F) varicosities, and (G) appendages on SCN neurons based on Golgi staining. n = 4–6 per group.

(H) Representative micrographs of mRFP-β-actin fluorescence in cultured SCN neurons from wild-type and *132/212* KO mice. Cultures were treated with BDNF (+BDNF) or vehicle (control) 24 hr before harvest. Red arrowheads indicate dendritic protrusions. Scale bar, 5 μm.

(I) Total protrusion density of mRFP-β-actin-transfected SCN neurons from wild-type and *132/212* KO mice, with or without BDNF treatment. n = 20–27 neurons per group.

All values represent mean ± SEM. *p < 0.05 versus wild-type (D–G) or as indicated (I).

protrusions, specifically varicosities and appendages, in the central SCN did not differ between genotypes (Figures 4F and 4G). Furthermore, simple spine and total protrusion density were not perturbed in the motor cortex of *132/212* KO mice under all photoperiods (Figures S4E–S4I), indicating that only selective brain regions are affected by *miR-132/212* ablation.

Figure 3. Analysis of the SCN Proteomes of Wild-Type and *132/212* KO Mice under Short Days: Implications for Neuronal Structure and mTOR Signaling

(A) Schematic overview of SILAC-based quantification of the SCN proteome of wild-type and *132/212* KO mice. SCN tissues from mice that were maintained under 8:16 hr L:D were harvested at four ZTs, spaced 6 hr apart, in which ZT 0 corresponds to lights on. Three neural cell lines were labeled by SILAC and mixed 1:1 with SCN protein lysates. Samples were processed and subjected to liquid chromatography-tandem mass spectrometry (LC-MS/MS) analysis.

(B) Venn diagram illustrating the overlap between the wild-type and *132/212* KO proteomes that exhibit time-of-day-dependent fluctuations under 8:16 hr L:D.

(C) FAT Gene Ontology enrichment analysis by DAVID based on biological process (BP). The 312 or 236 proteins that were time-of-day dependent only in the wild-type or only in the *132/212* KO SCN proteomes, respectively, were analyzed.

(D and E) Hierarchical cluster analysis of those (D) 365 time-of-day-dependent proteins in the wild-type SCN and (E) 289 time-of-day-dependent proteins in the *132/212* KO SCN in both genotypes. Note the dampened expression in the *132/212* KO SCN in (D) and in the wild-type SCN in (E).

(F) Canonical pathway analysis by IPA of the time-of-day wild-type and *132/212* KO SCN proteomes. The top ten ranked pathways are listed with corresponding −log(p value).

(G and H) Representative micrographs of phospho-S6 ribosomal protein (Ser240/244) abundance in the SCN of wild-type and *132/212* KO mice under (G) 8:16 hr L:D or (H) 16:8 hr L:D. Scale bar, 100 μm.

(I and J) Quantification of phospho-S6-IR intensity (in a.u.) in the whole SCN under (I) 8:16 hr L:D or (J) 16:8 hr L:D. n = 3–4 per group.

All values represent mean ± SEM. *p < 0.05 versus wild-type.

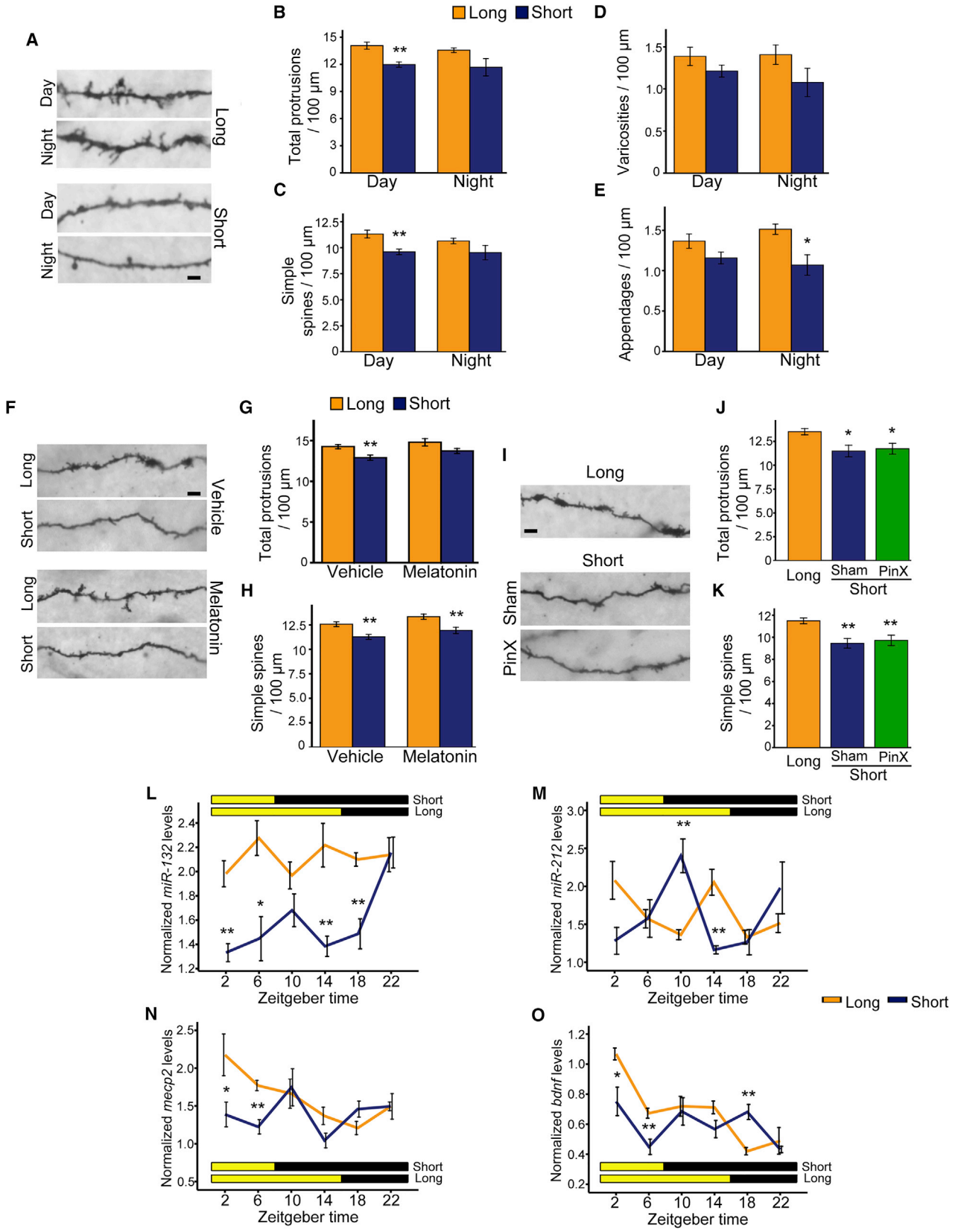

(legend on next page)

We confirmed our in vivo findings using a dispersed SCN neuronal culture model. Cultures prepared from *132/212* KO pups reared in 12:12 hr L:D had a lower density of dendritic protrusions compared with WT cultures (Figures 4H and 4I). The numbers of primary neurites and branching points were comparable between genotypes (Figures S4J and S4K). Treatment with BDNF for 24 hr rescued the defect in protrusion density of *132/212* KO SCN neurons (Figures 4H and 4I). Altogether, our data show that lack of miR-132/212 suppresses dendritic spine formation on SCN neurons, potentially through a BDNF-dependent mechanism.

Photoperiodic Regulation of miR-132/212 Expression and Dendritic Morphology in the SCN of Syrian Hamsters, a Seasonal Rodent

Ablation of *miR-132/212* in mice reduces the density of simple spines and total protrusions on SCN neurons, although this effect was observed under all photoperiods. However, closer inspection of the data revealed that the composition of dendritic protrusions varied according to photoperiod: long days correlated with greater numbers of simple spines and fewer varicosities and appendages in WT SCN (Figures 4E–4G). To explore further the effects of day length on *miR-132/212* expression and dendritic morphology in the SCN, we employed a rodent species that exhibits prominent seasonal changes in behavior and physiology, the Syrian hamster (*Mesocricetus auratus*). Male hamsters housed under 8:16 hr L:D (short day [SD]) for 7 weeks, sufficient to induce SD-dependent weight gain (Figure S5A), had reduced densities of total and subtype-specific protrusions in all regions of the SCN when compared to 16:8 hr L:D (long day [LD])-exposed hamsters (Figures 5B–5E, S5B, and S5C). Specifically, total protrusion and simple spine density were significantly lower in the central SCN of SD hamsters during the middle of the day (Figures 5B and 5C) and in the rostral and caudal SCN during the middle of the night (Figures S5B and S5C). Day length effects on protrusion density were not evident in the motor cortex (Figures S5D and S5E).

To rule out melatonin (MEL) as the mediator of day-length-dependent changes in protrusion density in the Syrian hamster SCN, we examined protrusion density of SCN neurons under two paradigms: (1) daily administration of MEL in the late day to mimic its release under SD (Figures 5F–5H) and (2) abolition of MEL production in SD-exposed hamsters by pinealectomy (PinX) (Figures 5I–5K). Daily MEL administration reduced testes weight of LD hamsters as expected (Figure S5F) but did not suppress total protrusion or simple spine density in these animals (Figures 5G and 5H). Conversely, pinealectomy had no effect on total protrusion or simple spine density in SD hamsters (Figures 5J and 5K). These data indicate that day-length-dependent variations in protrusion density in the hamster SCN are mediated by mechanisms other than melatonin signaling, which is absent in mice of the C57BL/6 background.

We found that the hamster SCN expressed both mature miR-132 and miR-212 and that miR-132 levels in particular were strongly dependent on day length. Both miRNAs were rhythmically expressed in the SCN of SD hamsters (Figures 5L and 5M). Under LD, levels of mature miR-132 were constitutively elevated and non-rhythmic (Figure 5L). Under both photoperiods, miR-212 rhythms seemed to track the light-dark transitions, peaking slightly before or after (Figure 5M). The correlation between low miR-132 levels and reduced protrusion density in the SCN of SD hamsters parallels our findings in the *132/212* KO mouse model. There was no consistent effect of day length on the abundance of miR-132 and miR-212 in the hamster cortex (Figures S5G and S5H). Overall, our results suggest that miR-132/212 has a physiologically relevant role in regulating seasonal changes in dendritic morphology of SCN neurons.

miR-132/212 Ablation Dysregulates BDNF and MeCP2 Expression in the SCN

Our results from dispersed SCN neuronal cultures suggest that the expression or activity of BDNF may be altered in *132/212* KO mice. BDNF is an upstream activator of the mTOR pathway and is transcriptionally regulated by MeCP2, a miR-132 target (Alvarez-Saavedra et al., 2011; Klein et al., 2007; Takei et al., 2004). Mutations in the X-linked gene MeCP2 underlies Rett syndrome, a neurological disorder afflicting females that is associated with dendritic spine dysgenesis (Jiang et al., 2013; Amir et al., 1999). In keeping with their potential relevance to seasonal changes in SCN dendritic morphology, we found evidence for photoperiod-dependent expression of *bdnf* and *mecp2* in the hamster SCN (Figures 5N and 5O). Both transcripts fluctuated with a robust circadian rhythm under LD (Figures 5N and 5O). Under SD, their daytime expression was significantly suppressed, reducing their oscillatory amplitude (Figures 5N and 5O). Day length had minimal effect on *mecp2* and *bdnf* expression in the hamster cortex (Figures S5I and S5J). We conclude that day length regulates expression of *bdnf* and *mecp2* in the hamster SCN, which in turn may contribute to changes in dendritic morphology.

We then examined *bdnf* expression in the SCN of *132/212* KO and WT mice under different photoperiods. The presence of exon IX (Figure 6A) or exon IV (Figure 6B) was used to quantify

Figure 5. Photoperiodic Regulation of Dendritic Protrusion Density and Gene Expression in the SCN of Syrian Hamsters

(A) Golgi-stained SCN neurons from Syrian hamsters maintained under a long (16:8 hr L:D) or short (8:16 hr L:D) photoperiod. Tissues were harvested mid-day or mid-night. Scale bar, 100 μm.

(B–E) Density of (B) total protrusions, (C) simple spines, (D) varicosities, and (E) appendages on hamster SCN neurons based on Golgi staining. n = 5 per group.

(F–K) Golgi-stained SCN neurons from Syrian hamsters maintained under a long or short photoperiod (F and I). (F) Hamsters received daily injections of melatonin or vehicle for the final 60 days under 16:8 hr L:D (long) or 8:16 hr L:D (short). (I) Hamsters underwent pinealectomy (PinX) or sham surgery before transfer to 8:16 hr L:D (short). Results were compared to non-surgerized hamsters under 14:10 hr L:D (long). Densities of (G and J) total protrusions and (H and K) simple spines on SCN neurons of hamsters that had (G and H) received daily melatonin injections or (J and K) undergone pinealectomy are shown. n = 7 per group.

(L–O) Quantitative RT-PCR analysis of the abundance of (L) mature miR-132, (M) mature miR-212, (N) *mecp2* transcripts, and (O) *bdnf* transcripts in the SCN of hamsters maintained under a long (16:8 hr L:D) or short (8:16 hr L:D) photoperiod. Colored bars indicate the L:D cycle. n = 5 per group.

All values represent mean ± SEM. *$p < 0.05$ and **$p < 0.01$ versus long photoperiod or vehicle control.

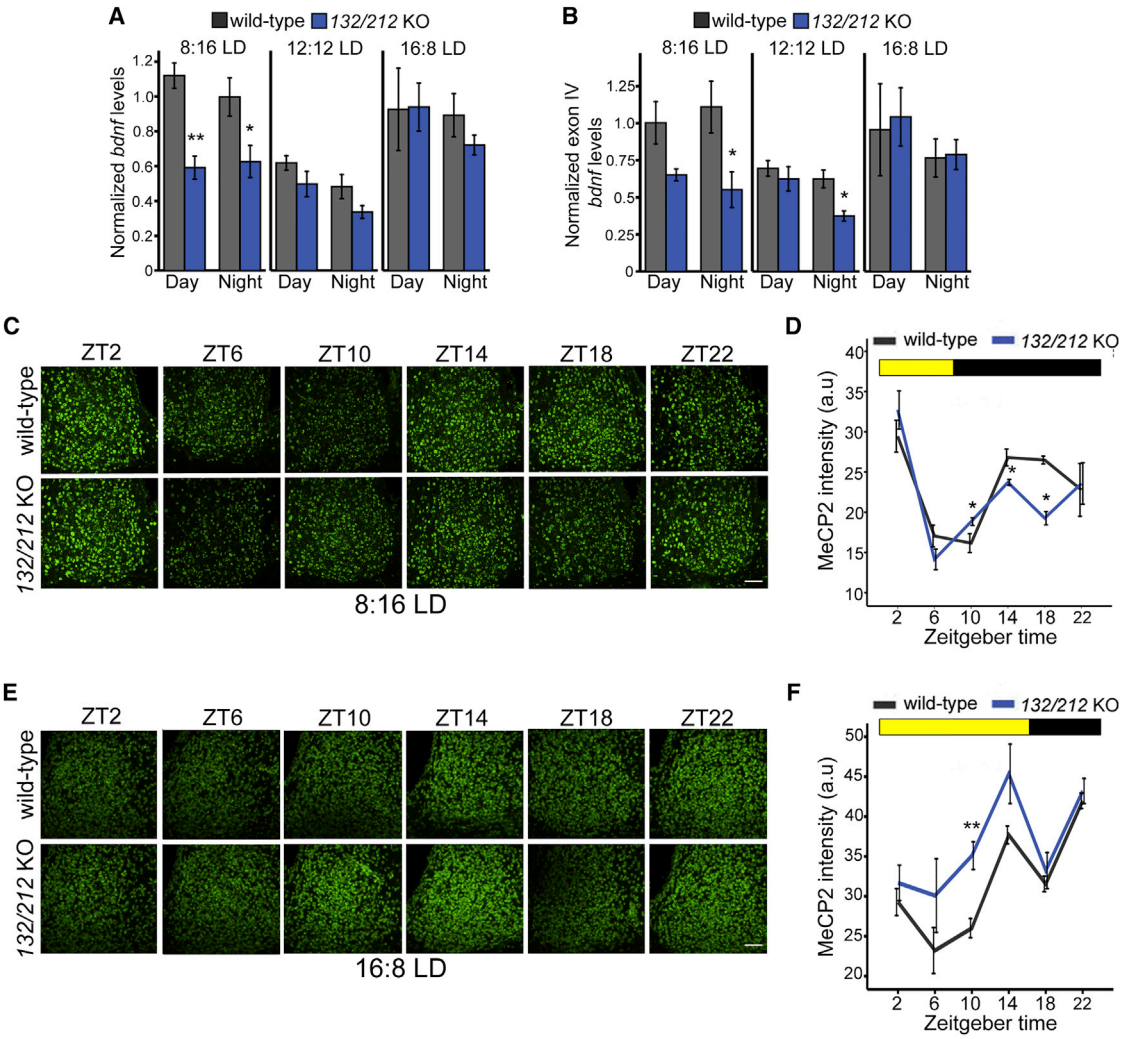

Figure 6. BDNF and MeCP2 Expression Are Dysregulated in the SCN of *miR-132/212*-Deficient Mice

(A and B) qRT-PCR analysis of the abundance of (A) all *bdnf* transcripts and (B) variants harboring exon IV in the SCN of wild-type and *132/212* KO mice maintained under 8:16, 12:12, or 16:8 hr L:D. Expression mid-day and mid-night was assessed. n = 4–6 per group.

(C–F) Representative micrographs of MeCP2 immunofluorescence in the SCN of wild-type and *132/212* KO mice maintained under (C) 8:16 hr L:D or (E) 16:8 hr L:D. Scale bar, 50 μm. Quantification of MeCP2-IR intensity in the whole SCN under (D) 8:16 hr L:D or (F) 16:8 hr L:D. Colored bars indicate the L:D cycle. n = 3–4 per group.

All values represent mean ± SEM. *p < 0.05 and **p < 0.01 versus wild-type.

levels of either total or neuronal activity- or MeCP2-dependent *bdnf* transcripts (Zhou et al., 2006), respectively. *miR-132/212* ablation significantly reduced levels of total *bdnf* transcripts under SD but had no effect under LD or 12:12 hr L:D (Figure 6A). Expression of exon IV was suppressed in the absence of *miR-132/212* under SD and during the night under 12:12 hr L:D (Figure 6B). These data suggest that decreased BDNF signaling may contribute to the reduction in spine density of *miR-132/212*-deficient SCN neurons, but only under short days.

The long transcript variant of *mecp2*, which is the dominant form in the brain, possesses a highly conserved and experimentally validated miR-132/212 binding site (Alvarez-Saavedra et al., 2011). Consistent with this, we found that MeCP2 protein rhythms in the SCN under different photoperiods were markedly perturbed in *132/212* KO mice (Figures 6C–6F, S6A, and S6B). Under 12:12 hr L:D (Figure S6B) and LD (Figure 6F), daytime expression of MeCP2 was significantly elevated in the SCN of *132/212* KO mice relative to WT. Under SD (Figure 6D), MeCP2 levels in the SCN were suppressed by *miR-132/212* ablation during the middle of the night but were unaltered in the day. These data suggest that perturbed temporal expression of MeCP2 in the SCN of *132/212* KO mice may underlie the generalized reduction in spine density of SCN neurons.

miR-132/212 Enhances Dendritic Spine Density via a MeCP2-Dependent Mechanism

To examine the role of MeCP2 in the protrusion density phenotype of *miR-32/212*-deficient SCN, we turned to our dispersed

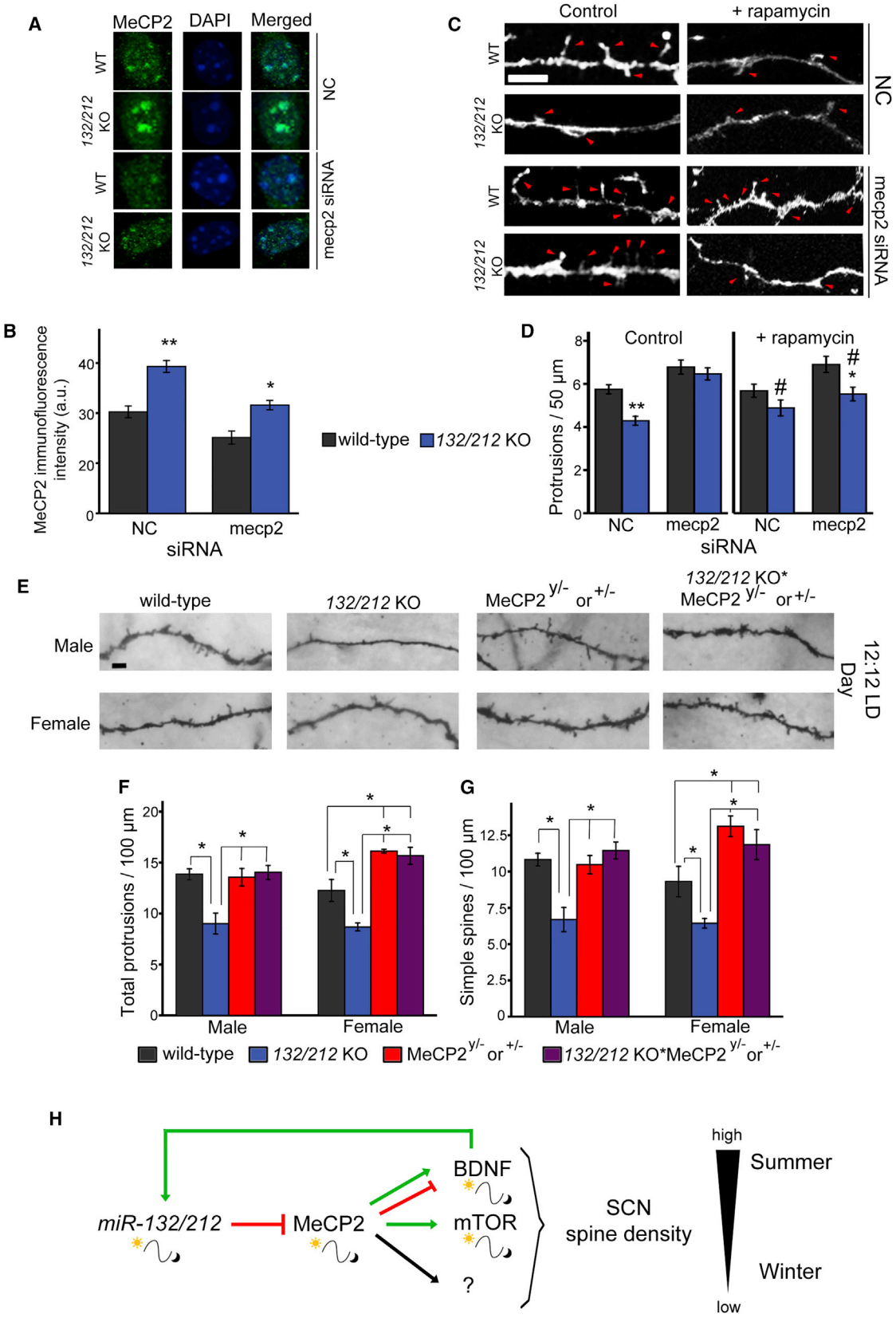

(legend on next page)

SCN neuronal culture system for initial insights. As expected, cellular levels of MeCP2 were elevated in *132/212* KO neurons relative to WT (Figures 7A, 7B, S6C, and S6D). Restoring the expression of MeCP2 to WT levels using a low dose of *mecp2* small interfering RNA (siRNA) (0.3 pg) (Figures S6C and S6D) resulted in full rescue of protrusion density of *132/212* KO SCN neurons to that observed in negative control (NC) siRNA-transfected WT neurons (Figures S6E and S6F). Protrusion density was enhanced even further in both WT and *132/212* KO SCN neurons (Figures 7C and 7D, control) when a higher dose of *mecp2* siRNA (10 pg) was used (Figures 7A and 7B). Moreover, the effects of MeCP2 on protrusion density were brain region specific: instead of elevating protrusion density, *mecp2* knockdown reduced it in cortical neurons, but only on a *miR-132/212* WT background (Figures S6G and S6H).

Next, we tested the involvement of the mTOR pathway by applying the mTOR inhibitor, rapamycin, to our dispersed SCN cultures for 24 hr (Figures 7C and 7D, +rapamycin). Rapamycin treatment modestly increased protrusion density of *132/212* KO SCN neurons, abolishing the effect of genotype (Figure 7D, NC lanes). In cultures transfected with *mecp2* siRNA (10 pg), rapamycin significantly reduced protrusion density of *132/212* KO SCN neurons, reinstating the difference between *132/212* KO and WT cultures (Figure 7D, mecp2 lanes). These data suggest that MeCP2-dependent rescue of protrusion density of *132/212* KO SCN neurons is dependent on mTOR signaling. They further suggest that there is an underlying perturbation of mTOR signaling in the SCN in the absence of miR-132/212.

Lastly, using the whole animal model, we examined the effects of *mecp2* ablation on the protrusion density phenotype of *132/212* KO mice (Figures 7E–7G, S6I, and S6J). Male and female mice were analyzed separately, because $mecp2^{-/y}$ male mice do not express MeCP2, whereas $mecp2^{+/-}$ female mice exhibit a mosaic expression pattern due to X inactivation ($mecp2^{-/-}$ females die in utero). In addition, analysis was performed on young (30–35 days old) mice before symptom onset. In male mice deficient for both *miR-132/212* and *mecp2*, total protrusion and simple spine density were restored to WT levels (Figures 7F and 7G). Furthermore, $mecp2^{-/y}$ and *132/212* KO/$mecp2^{-/y}$ male mice were phenotypically indistinguishable (Figures 7F and 7G). In female mice, regardless of *miR-132/212* status, *mecp2* heterozygosity markedly increased total protrusion and simple spine density to levels beyond those observed in WT (Figures 7F and 7G). Similar effects were observed for the density of appendages (Figure S6J), but not varicosities (Figure S6I). Collectively, our data show that *miR-132/212* ablation suppresses dendritic spinogenesis of SCN neurons through MeCP2-dependent mechanisms.

DISCUSSION

The SCN not only encodes circadian time but also is widely believed to encode day length information to regulate seasonal rhythms in behavior and physiology. Plasticity of the SCN has been proposed as an underlying mechanism for seasonal timekeeping. However, insights are scarce regarding the role of structural plasticity and the identities of specific molecular players in seasonal adaptation of the SCN network.

In this study, we show that *miR-132/212* ablation alters behavioral entrainment to seasonal photoperiods and non-24 hr cycles, as well as adaptive changes in the SCN clock to day length variation. Specifically, *132/212* KO mice entrain more efficiently to short days and <24 hr cycles and less efficiently to long days and >24 hr cycles. These behavioral phenotypes coincide with enhanced amplitude of PER2 rhythms in the SCN under short days and reduced phase separation of PER2 rhythms along the rostro-caudal axis of the SCN under long days. Photoperiodic regulation of *bdnf* expression, MECP2 rhythms, and mTOR activity were also perturbed in the SCN of *132/212* KO mice. Dysregulation of these spinogenesis-related factors is accompanied by a reduction in dendritic spine density of *miR-132/212*-deficient SCN neurons. In Syrian hamsters, the SCN adapts to changes in day length by altering SCN neuronal spine density in a melatonin-independent manner and the temporal expression profiles of miR-132, miR-212, *mecp2*, and *bdnf*. Genetic ablation of *mecp2* in mice fully restores spine density of *miR-132/212*-deficient SCN neurons. Altogether, these findings show that miR-132/212 regulates the capacity of the SCN to encode seasonal time by controlling dendritic morphology through a MeCP2-dependent mechanism.

Using acute antisense knockdown and transgenic overexpression of miR-132, we previously showed that miR-132 inhibits light-induced phase delays (Cheng et al., 2007; Alvarez-Saavedra et al., 2011). However, based on PRC analysis, *miR-132/212* KO mice do not exhibit any deficit in acute photic resetting. One possibility is that miR-132 and miR-212 have antagonistic roles in photic resetting, leading to a net zero effect when both are ablated. Alternatively, global deletion of *miR-132/212* throughout development may elicit compensatory changes that help to preserve the phase-shifting response.

Figure 7. MECP2 Depletion Rescues the Effects of *miR-132/212* Ablation on Dendritic Spine Formation

(A–D) Representative micrographs of (A) MeCP2 immunofluorescence (green) and (C) mRFP-β-actin fluorescence (white) in SCN neuronal cultures prepared from WT and *132/212* KO mice and co-transfected with 10 pg of *mecp2* siRNA or negative control (NC) siRNA. DAPI (blue) was used as a nuclear stain. For (C), cultures were treated with vehicle (control) or rapamycin (+rapamycin) 24 hr before harvest. Red arrowheads indicate dendritic protrusions. (B) Cellular MeCP2 intensity in wild-type and *132/212* KO SCN neuronal cultures from (A). (D) Total protrusion density of SCN neuronal cultures from (C). n = 20–43 neurons per group.

(E) Golgi-stained SCN neurons from age-matched male and female mice carrying the *miR-132/212* null and/or *Mecp2* null allele or alleles. Mice were maintained under 12:12 hr L:D before tissue harvest.

(F and G) Density of (F) total protrusions and (G) simple spines on SCN neurons based on Golgi staining in (E). n = 4–6 per group.

(H) Model depicting the role of miR-132/212 in dendritic morphogenesis of the SCN and implications for seasonal adaptation. *miR-132/212* expression is regulated by day length. Under short (winter) days, low *miR-132/212* expression leads to altered MeCP2 rhythms in the SCN. MeCP2 acts on downstream pathways, including BDNF, mTOR, and as-yet-unidentified mechanisms, to reduce SCN spine density in the winter. Conversely, the SCN adapts to summer days by increasing spine density.

All values represent mean ± SEM. *$p < 0.05$, *$p < 0.01$ versus WT (B and D) or as indicated (F and G). #$p < 0.05$ versus control.

Despite the lack of an acute resetting phenotype, when challenged with non-24 hr cycles, *132/212* KO mice have difficulty entraining to long T-cycles and entrain more effectively to short T-cycles. This stands in contrast to a previous study showing that the PRC accurately predicts entrainment to T-cycles and responsiveness to LL (Pendergast et al., 2010). However, the neural and molecular mechanisms underlying T-cycle entrainment and associated period aftereffects remain understudied and obscure and may not be identical to the mechanisms that govern acute resetting. For example, Azzi et al. (2014) showed that short T-cycles trigger persistent, genome-wide changes in DNA methylation in the SCN, an effect not previously examined in light pulse (LP) paradigms. In addition to potential epigenetic mechanisms, circuit-level properties of the SCN may dictate the ability of the SCN to entrain to extreme cycle lengths (Abraham et al., 2010), perhaps to a greater extent than its responsiveness to acute light stimuli. As discussed later, there are hints that the SCN neuronal network of *132/212* KO mice is more rigid or strongly coupled.

Our study also revealed that *miR-132/212* ablation alters entrainment to different day lengths. *132/212* KO mice entrain more slowly to long, but not short, days. However, their daily activity onset under short, but not long, days differs markedly from that of WT mice, matching closely the onset of darkness. Previous studies have demonstrated that the SCN encodes variations in day length by altering its network organization (Meijer et al., 2010). Exposure to long days leads to phase separation between SCN subregions along the rostral-caudal or dorsal-ventral axis, whereas SCN subregions are highly synchronized to one another under short days (Myung et al., 2015; Inagaki et al., 2007; VanderLeest et al., 2007; Hazlerigg et al., 2005). Based on PER2 expression analysis, it would appear that rhythms across the rostral-caudal axis of *miR-132/212*-deficient SCN remain tightly coupled under long days and have heightened amplitudes (possibly because of greater synchrony) under short days.

Other lines of evidence support the view that coupling is inherently stronger in *miR-132/212*-deficient SCN regardless of photoperiod. First, constant light, which desynchronizes SCN neurons (Ohta et al., 2005), does not lengthen the period of *132/212* KO mice to the same extent as it does WT. Second, enhanced amplitude of PER2 cycling was observed in SCN explants and in dark-adapted mice that were previously maintained under 12:12 hr L:D. While this increase in amplitude could be due to cell-autonomous mechanisms—we previously showed that *Period2* transcription is enhanced by MeCP2 (Alvarez-Saavedra et al., 2011)—it could also be explained by greater intra-SCN synchrony. Future studies should directly address the role of miR-132/212 in interneuronal coupling within the SCN.

Morphometric analysis revealed that dendritic spine density of SCN neurons is reduced in *132/212* KO mice, providing a potential structural basis for the myriad behavioral and molecular phenotypes that rely on altered SCN network organization. This is in line with previous reports documenting the role of miR-132 as a positive regulator of dendritic spinogenesis in the hippocampus and visual cortex (Mellios et al., 2011; Magill et al., 2010), although not all brain regions exhibit a reduction in spine density when *miR-132/212* is globally deleted from embryonic development onward (this study). The spine density reduction was observed predominantly in the central SCN under all photoperiods. This, combined with the lack of phenotype in DD period and acute resetting, suggests that the spine deficit does not have behavioral repercussions unless the circadian system is challenged with more extreme light conditions.

The hamster studies affirm the relevance of spine density changes and miR-132/212 expression to seasonal adaptation of the SCN. Both are heavily dependent on the photoperiod, with short days promoting the downregulation of dendritic spine density and levels of mature miR-132 in the SCN. Spine density of hamster SCN neurons was not affected by manipulations of melatonin signaling, even as other physiological parameters such as gonadal regression were affected. Therefore, we believe that reduced spine density in SD hamsters is a direct consequence of lower miR-132 expression, not merely a correlation. The expression of miR-132 and miR-212 in the hamster SCN is not mirrored under different photoperiods. Unlike miR-132, miR-212 is rhythmic under both LD and SD, and its expression appears to track the light-dark transitions. The dichotomy between the expression profiles of miR-132 and those of miR-212 raises intriguing questions regarding their relative contributions to seasonal changes in, and day length encoding by, the SCN.

We show that MeCP2 mediates the effects of *miR-132/212* ablation on dendritic spine density of SCN neurons. Expression of MeCP2 in the SCN is both rhythmic and photoperiod dependent. *132/212* KO mice have perturbed MeCP2 rhythms under all photoperiods, in particular elevated expression under 12:12 and 16:8 hr L:D. Complete ablation of *Mecp2* in male mice counters the effects of *miR-132/212* deletion on spine density of SCN neurons, restoring it to WT levels. Similar results were found when we assessed the effects of *Mecp2* knockdown on spine density in dispersed SCN cultures. The spine density of SCN neurons from *Mecp2*$^{+/-}$ female mice, which have mixed populations of wild-type MeCP2 and MeCP2 null cells throughout the brain, is well above WT levels, suggesting that MeCP2 regulates spine density through both cell-autonomous and cell-non-autonomous mechanisms. Despite an extensive literature investigating the role of MeCP2 in dendritic morphogenesis, the effects of MeCP2 appear to be complex, varying as a function of gene dosage, brain region, and time since MeCP2 misexpression. For example, 2-fold overexpression of MeCP2 has been shown to both increase and decrease spine density in pyramidal neurons of the somatosensory cortex (albeit only in young mice) (Jiang et al., 2013) and hippocampus (Cheng et al., 2014; Chapleau et al., 2009), respectively.

Basal and photoperiodic regulation of dendritic spine density of SCN neurons are likely influenced by BDNF and mTOR signaling, which form a functional network with miR-132/212 and MeCP2 (Ricciardi et al., 2011; Klein et al., 2007; Zhou et al., 2006). However, they cannot account entirely for the spine density phenotype of *miR-132/212*-deficient SCN. Even though hamsters and *132/212* KO mice show suppressed *bdnf* expression, along with reduced spine density, under SD, in the *132/212* KO mouse model, *bdnf* expression is normal under LD, yet spine density remains lower than WT. The cell culture model indicates that BDNF treatment can acutely increase spine density of *miR-132/212*-deficient SCN neurons. With respect to mTOR, *132/212*

KO mice exhibit altered mTOR activity rhythms in the SCN under 12:12 and 8:16 hr L:D. However, the in vitro effects of rapamycin are paradoxical, elevating spine density of SCN neurons in the absence of *miR-132/212* but suppressing it when *mecp2* is knocked down on the *132/212* KO background. Still, the cell culture system cannot recapitulate all in vivo conditions, including the effects of SCN network organization and photoperiod. It suggests that BDNF and/or mTOR can contribute to miR-132/212-dependent dendritic spinogenesis but only under specific contexts that take into account the status of the other components of this functional network, other genetic perturbations, and photoperiod.

Figure 7H depicts our current working model of miR-132/212's role in seasonal adaptation of the SCN. Shorter days in the winter downregulate the expression of *miR-132/212* in the SCN, which in turn alters the rhythmic expression of its direct target, MeCP2. MeCP2 works through different downstream mechanisms that, altogether, mediate the negative effects of miR-132/212 downregulation on dendritic spinogenesis of SCN neurons. These mechanisms include BDNF and mTOR signaling. We speculate that there may also be an epigenetic contribution by MeCP2 to photoperiod-dependent spinogenesis in the SCN. We further speculate that greater spine density on SCN neurons under long days allows SCN subregions to uncouple or desynchronize from one another, potentially by increasing repulsive coupling forces that have been reported in the literature (Myung et al., 2015).

EXPERIMENTAL PROCEDURES

Ethics Statement

Animal handling and experiments were performed at the University of Toronto Mississauga (UTM) Animal Facility and were approved by the UTM animal care committee, complying with institutional guidelines and the Canadian Council on Animal Care. Pinealectomy experiments were performed at the Université de Strasbourg with approval by the Comité d'Ethique en Matière d'Expérimentation Animale (CREMEAS) and in accordance with the French national law for animal experimentation (No. 2016022211221007) and the rules of the European Communities Council Directive of November 24, 1986 (86/609/EEC).

Animals

miR-132/212 germline knockout mice were obtained from R. Goodman. C57BL/6J, mPER2::LUC (B6.129S6-*Per2*^{tm1Jt}/J), and *Mecp2*$^{+/-}$ (B6.129P2(C)-*Mecp2*$^{tm1.1Bird}$/J) mice were purchased from The Jackson Laboratory. Six-week-old male golden Syrian hamsters (*Mesocricetus auratus*) were purchased from Charles River Laboratories and Janvier Labs.

Behavioral Analyses

Male mice (5–10 weeks old) were individually housed in running-wheel cages within ventilated, light-tight cabinets under computer-controlled lighting schedules (Phenome Technologies). Light intensity was 30 lux (0.38 μE) at cage level unless otherwise indicated. Wheel revolutions were recorded and analyzed using ClockLab software (Actimetrics). For PRC analysis, mice received a 15 min light pulse (LP: 40 lux, 0.50 μE) at the designated CT after ~2 weeks in DD. For T-cycle experiments, mice experienced once-weekly changes in the T-cycle by ±0.5 hr steps from T24 to T22 or T26. For circadian aftereffects, mice experienced daily changes in the T-cycle by ±10 min steps from T24 to T22 or T26 and afterward were released into DD. For photoperiod experiments, mice were transferred abruptly from 12:12 to 8:16 or 16:8 hr L:D and maintained on the new schedule for 3 weeks. For LL experiments, mice were transferred to dim LL (30 lux) for 3 weeks and then to bright LL (100 lux, 1.24 μE) for 3 weeks. Period was measured with software-fitted regression lines and χ^2 periodogram. Phase shifts were measured as the displacement between two regression lines fitted through activity onsets before and after a LP. Phase angles of entrainment were measured by calculating the difference between onset of activity and lights-off.

Pinealectomy and Melatonin Injections

Male hamsters raised under 14:10 hr L:D were anesthetized, and pinealectomy or sham surgery was performed as described (Hoffman and Reiter, 1965). After recovery, animals were transferred to 8:16 hr L:D for 7 weeks before tissue harvest. For MEL injections, hamsters were housed under 8:16 or 16:8 hr L:D for 80 days and received daily subcutaneous injections of melatonin (50 μg, Toronto Research Chemicals) or vehicle ~1.5–2 hr before lights-off on days 21–80. After the last injection, tissues were harvested 4 hr after lights-off.

Tissue Harvest

Male and female mice, aged 4–8 weeks, and male hamsters were killed by cervical dislocation and decapitation (after isoflurane or Zoletil anesthesia), respectively, under white light or dim red light as appropriate. Coronal sections were obtained with a vibratome or brain matrix. For immunostaining, coronal sections were fixed in 4% paraformaldehyde (PFA) for 6 hr and cryoprotected in 30% sucrose solution. For all other experiments, SCN tissues were dissected from the whole brain using microscissors (RNA experiments) or from 800 μm coronal sections, frozen quickly on dry ice, and stored at −80°C until use.

RNA Extraction and RT-PCR

Total RNA was isolated using the miRCURY Isolation Kit (Exiqon) or TRIzol Reagent (Invitrogen-Thermo Scientific). For miRNA analysis, cDNA was synthesized with the Universal cDNA Synthesis Kit II (Exiqon) and qPCR was performed with the ExiLENT SYBR Green kit using microRNA locked nucleic acid (LNA) miR-132, miR-212, and miR-191 PCR primer sets (Exiqon). For mRNA analysis, cDNA was synthesized with SuperScript IV Reverse Transcriptase (Invitrogen), and RT-PCR was performed using SsoFast Evagreen Supermix (Bio-Rad). Data were normalized to *gapdh* (for *bdnf* and *mecp2*) or miR-191 (for miR-132 and miR-212), the latter a commonly used reference miRNA (Peltier and Latham, 2008) that exhibited minimal time-of-day or photoperiod dependency in its expression in the hamster SCN.

Golgi Staining

Golgi stains were performed using the Rapid GolgiStain Kit (FD NeuroTechnologies).

Dispersed SCN Neuronal Cultures and Transfection

Cortical and SCN neuronal cultures were prepared from post-natal day (P) 0 and P4–P6 mouse pups, respectively. Tissues were trypsinized, triturated, and plated onto poly-D-lysine-coated coverslips. At day in vitro (DIV) 4, cells were transfected with pCAGGS-mRFP-β-actin and *MeCP2* or NC siRNA (ON-TARGETplus SMARTpool, GE Dharmacon Technologies) using Lipofectamine 3000 (Invitrogen). Where specified, cultures were treated with 50 ng/mL BDNF (Novoprotein) or 10 nM rapamycin (Tocris) on DIV 5. At 48 hr post-transfection, cells were fixed with 4% PFA and, if needed, processed by immunocytochemistry using the MeCP2 antibody before mounting.

Image Acquisition and Quantification

Images were acquired using a Zeiss Axio Observer Z1 inverted microscope, equipped with a laser scanning microscope (LSM) 700 module for confocal images, and an AxioCam MRm Rev.3 monochromatic digital camera (Zeiss) for bright-field pictures. Images were analyzed using ImageJ software. The "free-hand" tool was used to outline the region of interest. The "measure" function was used to obtain the mean optical density, minus background measurements from an adjacent, non-immunoreactive region. For cell counts, images were converted to binary and processed with the Watershed filter, and cells were counted with the "analyze particle" function. Cell density was calculated by measuring the area. For Golgi staining, multiple optical z planes were obtained at 20×. Stained neuronal projections were traced and measured. Protrusions were classified as simple spines (≤3 μm length), appendages (>3 μm), and varicosities. For MeCP2 immunostaining, 40× or 63× confocal

images were obtained, and fluorescence intensity of the SCN or individual cell nuclei was measured. Monomeric red fluorescent protein (mRFP)-β-actin fluorescence was imaged at 63×, with a 1 μm distance between z planes and eight averages per pixel. Dendritic protrusions were counted. Protrusion density was calculated by dividing the number of protrusions by dendritic length.

Mass Spectrometry

Cell Culture

Neuro2A cells (American Type Culture Collection), adult mouse hypothalamus cell line mHypoA-2/28 (CLU188, CELLutions Biosystems), and adult mouse hypothalamus cell mHypoA-SCN mix (CLU497, CELLutions Biosystems) were grown in SILAC media as described (Chiang et al., 2014).

Sample Processing

SCN protein lysates were processed using the filter-aided sample preparation (FASP) method as described (Wiśniewski et al., 2009), with some modifications. SCN lysates (45 μg of proteins) and heavy SILAC-labeled cell lysates (15 μg from each cell line) were mixed at a 1:1 ratio before transfer onto the filter. After sample processing on the filter devices, peptides were eluted and fractionated using an in-house constructed strong cation exchange (SCX) column with five pH fractions (pH 4.0, 6.0, 8.0, 10.0, and 12.0). Fractionated samples were desalted using in-house C18 desalting cartridges and dried in a SpeedVac before liquid chromatography-mass spectrometry (LC-MS) analysis.

LC-MS Analyses

Peptide mixtures were analyzed by high-performance liquid chromatography/electrospray ionization-tandem mass spectrometry (HPLC-ESI-MS/MS). The HPLC-ESI-MS/MS consisted of an automated Ekspert NanoLC 400 system (Eksigent) coupled with an LTQ Velos Pro Orbitrap Elite mass spectrometer (Thermo Fisher Scientific) equipped with a nanoelectrospray interface operated in positive ion mode. LC-MS analysis was conducted as described (Chiang et al., 2014) with modification to some parameters (see Supplemental Information).

Database Search and Bioinformatic Analysis

Database search was conducted as described (Chiang et al., 2014) with modification to some parameters (see Supplemental Information). The protein-group file was imported into Perseus (v.1.5.2.4) for data statistical analysis. The MS raw dataset (4,569 proteins) was filtered to generate a stringently quantified dataset of 2,334 proteins, which includes only proteins with a minimum peptide ratio count of 2 and quantification values in at least 16 of 32 independent SCN samples (n = 4 per group). Pairwise Pearson's correlation analysis yielded high r values (>0.90) for all comparisons, indicating good reproducibility within the dataset. The stringent dataset was analyzed by one-way ANOVA to identify proteins from the wild-type or *132/212* KO proteome that exhibit statistically significant ($p < 0.05$) alterations across the 24 hr cycle. Hierarchical clustering analysis was achieved by clustering the median of logarithmized values for the normalized light/heavy (L/H) ratio of each significantly altered protein profile after *Z* score normalization of the data within Euclidean distances. Analysis of canonical pathways by Ingenuity Pathways Analysis (IPA) (Ingenuity Systems) was performed with a p value of 0.05. Bioinformatics Gene Ontology (GO) analyses were achieved using the Database for Annotation, Visualization, and Integrated Discovery (DAVID) Bioinformatics Resources (https://david.ncifcrf.gov/). Fisher's exact test was used to extract the FAT results that were significantly enriched ($p < 0.05$) in each time-of-day proteome, relative to the stringent dataset as background in each GO term.

Statistical Analyses

Student's t tests (with Bonferroni correction for multiple comparison where needed), χ^2 tests, one-way ANOVA, and Fisher's least significance difference (LSD) were performed using SPSS Statistics 20 software (IBM), with α set at 0.05.

ACCESSION NUMBERS

The accession number for the mass spectrometry proteomics data reported in this paper is PRIDE: PXD003635 (Vizcaíno et al., 2013).

SUPPLEMENTAL INFORMATION

Supplemental Information includes Supplemental Experimental Procedures, six figures, and one table and can be found with this article online at http://dx.doi.org/10.1016/j.celrep.2017.03.057.

AUTHOR CONTRIBUTIONS

H.-Y.M.C. conceived the study. H.-Y.M.C. and L.M.-V. prepared the manuscript. C.-K.C. performed and analyzed MS data. D.F. assisted in MS experiments and data analysis. J.L.K.O., S.H., A.H.C., P.B.-C., M.F., C.L., and M.G.M. assisted in image acquisition and quantification. P.Z. performed T-cycle and masking experiments. B.B. and V.S. performed pinealectomies and harvested tissues. S.T.M. and R.H.G. developed and provided *miR-132/212* KO mice. M.M.H. provided support for behavioral experiments. L.M.-V. performed all other experiments and data analysis.

ACKNOWLEDGMENTS

The authors thank D. Weaver (PER2 and BMAL1 antibodies), S. Reppert (PER1 antibodies), G. Wayman (pCAGGS-mRFP-β-actin construct), A. Monks (use of cryostat), and R. Abdelmegid and T. Piekut (technical assistance). The authors also thank A. Senatore and J. Levine for helpful comments on the manuscript. This work was supported by operating grants to H.-Y.M.C. and D.F. from the Canadian Institute of Health Research (CIHR) (MOP#86549 and MOP#126090) and the Natural Sciences and Engineering Research Council (NSERC) of Canada (RGPIN386495-11). H.-Y.M.C. is a Tier II Canada Research Chair (CRC) in Molecular Genetics of Biological Clocks, and D.F. is a Tier I CRC in Proteomics and Systems Biology. R.H.G. is supported by funding from NIMH NIH HHS (MH094416). L.M.-V. is supported by a graduate scholarship from the Consejo Nacional de Ciencia y Tecnologia (CONACyT) of Mexico. S.H., A.H.C., P.B.-C., and M.F. are supported by NSERC Canada Graduate Scholarships.

Received: March 7, 2016
Revised: January 11, 2017
Accepted: March 17, 2017
Published: April 18, 2017

REFERENCES

Abraham, U., Granada, A.E., Westermark, P.O., Heine, M., Kramer, A., and Herzel, H. (2010). Coupling governs entrainment range of circadian clocks. Mol. Syst. Biol. *6*, 438.

Alvarez-Saavedra, M., Antoun, G., Yanagiya, A., Oliva-Hernandez, R., Cornejo-Palma, D., Perez-Iratxeta, C., Sonenberg, N., and Cheng, H.Y. (2011). miRNA-132 orchestrates chromatin remodeling and translational control of the circadian clock. Hum. Mol. Genet. *20*, 731–751.

Amir, R.E., Van den Veyver, I.B., Wan, M., Tran, C.Q., Francke, U., and Zoghbi, H.Y. (1999). Rett syndrome is caused by mutations in X-linked MECP2, encoding methyl-CpG-binding protein 2. Nat. Genet. *23*, 185–188.

Aton, S.J., Block, G.D., Tei, H., Yamazaki, S., and Herzog, E.D. (2004). Plasticity of circadian behavior and the suprachiasmatic nucleus following exposure to non-24-hour light cycles. J. Biol. Rhythms *19*, 198–207.

Azzi, A., Dallmann, R., Casserly, A., Rehrauer, H., Patrignani, A., Maier, B., Kramer, A., and Brown, S.A. (2014). Circadian behavior is light-reprogrammed by plastic DNA methylation. Nat. Neurosci. *17*, 377–382.

Chapleau, C.A., Calfa, G.D., Lane, M.C., Albertson, A.J., Larimore, J.L., Kudo, S., Armstrong, D.L., Percy, A.K., and Pozzo-Miller, L. (2009). Dendritic spine pathologies in hippocampal pyramidal neurons from Rett syndrome brain and after expression of Rett-associated MECP2 mutations. Neurobiol. Dis. *35*, 219–233.

Chen, R., D'Alessandro, M., and Lee, C. (2013). miRNAs are required for generating a time delay critical for the circadian oscillator. Curr. Biol. *23*, 1959–1968.

Cheng, H.Y., Papp, J.W., Varlamova, O., Dziema, H., Russell, B., Curfman, J.P., Nakazawa, T., Shimizu, K., Okamura, H., Impey, S., and Obrietan, K. (2007). microRNA modulation of circadian-clock period and entrainment. Neuron *54*, 813–829.

Cheng, T.-L., Wang, Z., Liao, Q., Zhu, Y., Zhou, W.-H., Xu, W., and Qiu, Z. (2014). MeCP2 suppresses nuclear microRNA processing and dendritic growth by regulating the DGCR8/Drosha complex. Dev. Cell *28*, 547–560.

Chiang, C.K., Mehta, N., Patel, A., Zhang, P., Ning, Z., Mayne, J., Sun, W.Y., Cheng, H.Y., and Figeys, D. (2014). The proteomic landscape of the suprachiasmatic nucleus clock reveals large-scale coordination of key biological processes. PLoS Genet. *10*, e1004695.

Gekakis, N., Staknis, D., Nguyen, H.B., Davis, F.C., Wilsbacher, L.D., King, D.P., Takahashi, J.S., and Weitz, C.J. (1998). Role of the CLOCK protein in the mammalian circadian mechanism. Science *280*, 1564–1569.

Hazlerigg, D.G., Ebling, F.J., and Johnston, J.D. (2005). Photoperiod differentially regulates gene expression rhythms in the rostral and caudal SCN. Curr. Biol. *15*, R449–R450.

Hoffman, R.A., and Reiter, R.J. (1965). Rapid pinealectomy in hamsters and other small rodents. Anat. Rec. *153*, 19–21.

Inagaki, N., Honma, S., Ono, D., Tanahashi, Y., and Honma, K. (2007). Separate oscillating cell groups in mouse suprachiasmatic nucleus couple photoperiodically to the onset and end of daily activity. Proc. Natl. Acad. Sci. USA *104*, 7664–7669.

Jiang, M., Ash, R.T., Baker, S.A., Suter, B., Ferguson, A., Park, J., Rudy, J., Torsky, S.P., Chao, H.T., Zoghbi, H.Y., and Smirnakis, S.M. (2013). Dendritic arborization and spine dynamics are abnormal in the mouse model of MECP2 duplication syndrome. J. Neurosci. *33*, 19518–19533.

Klein, M.E., Lioy, D.T., Ma, L., Impey, S., Mandel, G., and Goodman, R.H. (2007). Homeostatic regulation of MeCP2 expression by a CREB-induced microRNA. Nat. Neurosci. *10*, 1513–1514.

Kume, K., Zylka, M.J., Sriram, S., Shearman, L.P., Weaver, D.R., Jin, X., Maywood, E.S., Hastings, M.H., and Reppert, S.M. (1999). mCRY1 and mCRY2 are essential components of the negative limb of the circadian clock feedback loop. Cell *98*, 193–205.

Magill, S.T., Cambronne, X.A., Luikart, B.W., Lioy, D.T., Leighton, B.H., Westbrook, G.L., Mandel, G., and Goodman, R.H. (2010). microRNA-132 regulates dendritic growth and arborization of newborn neurons in the adult hippocampus. Proc. Natl. Acad. Sci. USA *107*, 20382–20387.

Meijer, J.H., Michel, S., Vanderleest, H.T., and Rohling, J.H. (2010). Daily and seasonal adaptation of the circadian clock requires plasticity of the SCN neuronal network. Eur. J. Neurosci. *32*, 2143–2151.

Mellios, N., Sugihara, H., Castro, J., Banerjee, A., Le, C., Kumar, A., Crawford, B., Strathmann, J., Tropea, D., Levine, S.S., et al. (2011). miR-132, an experience-dependent microRNA, is essential for visual cortex plasticity. Nat. Neurosci. *14*, 1240–1242.

Myung, J., Hong, S., DeWoskin, D., De Schutter, E., Forger, D.B., and Takumi, T. (2015). GABA-mediated repulsive coupling between circadian clock neurons in the SCN encodes seasonal time. Proc. Natl. Acad. Sci. USA *112*, E3920–E3929.

Ohta, H., Yamazaki, S., and McMahon, D.G. (2005). Constant light desynchronizes mammalian clock neurons. Nat. Neurosci. *8*, 267–269.

Peltier, H.J., and Latham, G.J. (2008). Normalization of microRNA expression levels in quantitative RT-PCR assays: identification of suitable reference RNA targets in normal and cancerous human solid tissues. RNA *14*, 844–852.

Pendergast, J.S., Friday, R.C., and Yamazaki, S. (2010). Photic entrainment of period mutant mice is predicted from their phase response curves. J. Neurosci. *30*, 12179–12184.

Pittendrigh, C.S., and Daan, S. (1976a). A functional analysis of circadian pacemakers in nocturnal rodents: I. The stability and lability of spontaneous frequency. J. Comp. Physiol. *106*, 223–252.

Pittendrigh, C.S., and Daan, S. (1976b). A functional analysis of circadian pacemakers in nocturnal rodents: IV. Entrainment: pacemaker as clock. J. Comp. Physiol. A Neuroethol. Sens. Neural Behav. Physiol. *106*, 291–331.

Ralph, M.R., Foster, R.G., Davis, F.C., and Menaker, M. (1990). Transplanted suprachiasmatic nucleus determines circadian period. Science *247*, 975–978.

Ricciardi, S., Boggio, E.M., Grosso, S., Lonetti, G., Forlani, G., Stefanelli, G., Calcagno, E., Morello, N., Landsberger, N., Biffo, S., et al. (2011). Reduced AKT/mTOR signaling and protein synthesis dysregulation in a Rett syndrome animal model. Hum. Mol. Genet. *20*, 1182–1196.

Shigeyoshi, Y., Taguchi, K., Yamamoto, S., Takekida, S., Yan, L., Tei, H., Moriya, T., Shibata, S., Loros, J.J., Dunlap, J.C., and Okamura, H. (1997). Light-induced resetting of a mammalian circadian clock is associated with rapid induction of the mPer1 transcript. Cell *91*, 1043–1053.

Sosniyenko, S., Hut, R.A., Daan, S., and Sumová, A. (2009). Influence of photoperiod duration and light-dark transitions on entrainment of Per1 and Per2 gene and protein expression in subdivisions of the mouse suprachiasmatic nucleus. Eur. J. Neurosci. *30*, 1802–1814.

Stephan, F.K., and Zucker, I. (1972). Circadian rhythms in drinking behavior and locomotor activity of rats are eliminated by hypothalamic lesions. Proc. Natl. Acad. Sci. USA *69*, 1583–1586.

Takei, N., Inamura, N., Kawamura, M., Namba, H., Hara, K., Yonezawa, K., and Nawa, H. (2004). Brain-derived neurotrophic factor induces mammalian target of rapamycin-dependent local activation of translation machinery and protein synthesis in neuronal dendrites. J. Neurosci. *24*, 9760–9769.

VanderLeest, H.T., Houben, T., Michel, S., Deboer, T., Albus, H., Vansteensel, M.J., Block, G.D., and Meijer, J.H. (2007). Seasonal encoding by the circadian pacemaker of the SCN. Curr. Biol. *17*, 468–473.

Vizcaíno, J.A., Côté, R.G., Csordas, A., Dianes, J.A., Fabregat, A., Foster, J.M., Griss, J., Alpi, E., Birim, M., Contell, J., et al. (2013). The PRoteomics IDEntifications (PRIDE) database and associated tools: status in 2013. Nucleic Acids Res. *41*, D1063–D1069.

Wanet, A., Tacheny, A., Arnould, T., and Renard, P. (2012). miR-212/132 expression and functions: within and beyond the neuronal compartment. Nucleic Acids Res. *40*, 4742–4753.

Wayman, G.A., Davare, M., Ando, H., Fortin, D., Varlamova, O., Cheng, H.Y., Marks, D., Obrietan, K., Soderling, T.R., Goodman, R.H., and Impey, S. (2008). An activity-regulated microRNA controls dendritic plasticity by down-regulating p250GAP. Proc. Natl. Acad. Sci. USA *105*, 9093–9098.

Welsh, D.K., Logothetis, D.E., Meister, M., and Reppert, S.M. (1995). Individual neurons dissociated from rat suprachiasmatic nucleus express independently phased circadian firing rhythms. Neuron *14*, 697–706.

Wiśniewski, J.R., Zougman, A., Nagaraj, N., and Mann, M. (2009). Universal sample preparation method for proteome analysis. Nat. Methods *6*, 359–362.

Yamaguchi, S., Isejima, H., Matsuo, T., Okura, R., Yagita, K., Kobayashi, M., and Okamura, H. (2003). Synchronization of cellular clocks in the suprachiasmatic nucleus. Science *302*, 1408–1412.

Zhou, Z., Hong, E.J., Cohen, S., Zhao, W.N., Ho, H.Y., Schmidt, L., Chen, W.G., Lin, Y., Savner, E., Griffith, E.C., et al. (2006). Brain-specific phosphorylation of MeCP2 regulates activity-dependent Bdnf transcription, dendritic growth, and spine maturation. Neuron *52*, 255–269.